Rock and Soil Mechanics

Volume 42 | Issue 8 Article 8

12-16-2021

Numerical simulation of grouting process in rock mass with rough fracture network based on corrected cubic law

Wei CUI
Key Laboratory of Earthquake Engineering Simulation and Seismic Resilience of China Earthquake Administration, Tianjin University, Tianjin 300350, China;

Li-xin WANG
State Key Laboratory of Hydraulic Engineering Simulation and Safety, Tianjin University, Tianjin 300350, China;

Zhi-an JIANG
Sinohydro Foundation Engineering Co., Ltd., Tianjin 301700, China

Chao WANG
Key Laboratory of Earthquake Engineering Simulation and Seismic Resilience of China Earthquake Administration, Tianjin University, Tianjin 300350, China;

See next page for additional authors

Custom Citation

CUI Wei, WANG Li-xin, JIANG Zhi-an, WANG Chao, WANG Xiao-hua, ZHANG She-rong, . Numerical simulation of grouting process in rock mass with rough fracture network based on corrected cubic law[J]. Rock and Soil Mechanics, 2021, 42(8): 2250-2258.

Numerical simulation of grouting process in rock mass with rough fracture network based on corrected cubic law

Authors

Wei CUI, Li-xin WANG, Zhi-an JIANG, Chao WANG, Xiao-hua WANG, and She-rong ZHANG

Rock and Soil Mechanics 2021 42(8): 2250−2258 ISSN 1000−7598
https: //doi.org/10.16285/j.rsm.2021.5007 rocksoilmech.researchcommons.org/journal

Numerical simulation of grouting process in rock mass with rough fracture network based on corrected cubic law

CUI Wei[1, 2], WANG Li-xin[1], JIANG Zhi-an[3], WANG Chao[1, 2], WANG Xiao-hua[1], ZHANG She-rong[1, 2]

1. State Key Laboratory of Hydraulic Engineering Simulation and Safety, Tianjin University, Tianjin 300350, China;
2. Key Laboratory of Earthquake Engineering Simulation and Seismic Resilience of China Earthquake Administration, Tianjin University, Tianjin 300350, China;
3. Sinohydro Foundation Engineering Co., Ltd., Tianjin 301700, China

Abstract: Due to the influence of fracture undulation, there is an obvious difference in the grout flow rule between the rock mass with rough fractures and the rock mass with existing results. Based on the parallel plate model of fluid flow in a single crack, a flow rule model of viscous fluid in a rough fracture was developed using a corrected cubic law. The derived results were agreed well with that from a single crack grouting test. Based on a discrete fracture network (DFN) model, the grouting process in a fractured rock mass was simulated and studied by changing the fracture network characteristics and the grouting pressure. The results show that the grouting diffusion volume is controlled by the permeability of rock mass, but the connectivity plays a key factor affecting the fluid diffusion process, which can affect the fluid diffusion in local areas. The increase of grouting pressure changes the slurry diffusion velocity, which can make the slurry easier to diffuse to the remote areas that far from the grouting point and those areas with poor local connectivity, however, excessive grouting pressure may cause the fracture opening and even lead to the rock mass failure.
Keywords: jointed rock mass; discrete fracture network; viscous fluid; grouting; numerical modeling; flow rule

1 Introduction

A large number of fractures are formed in the rock foundation because of the geological movement for hundreds of millions of years[1−2]. The existence of fractures has an important influence on the mechanical properties of rock masses and fluid flow in the rock masses, which seriously affects the safety of rock construction projects. To solve this issue, grouting materials can be used to infill the micro-fissures within the rock mass, which assists the rock mass to become an integrated body[3−4]. Recently, rock fissure grouting has been made great progress in new techniques and new materials, however, the studies of the grouting process and diffusion mechanism are still incomplete, and its related theories lag far behind the requirements of grouting design and field construction. Because there are many difficulties in the field and laboratory tests, numerical modelling is in turn to be an important method for studying rock grouting[5], among which the law of grout flow in a single fracture is the very basis for numerical simulation. Ruan[6−7] developed a single fracture grouting diffusion model based on the time-varying law of slurry viscosity. Gustafson et al[8] developed an analytical solution for the diffusion and flow of Bingham fluid in a pair of smooth parallel plates, which served as a theoretical basis for the application of real-time grouting control method in rock grouting engineering[9]. Gao et al[10] built a single-fracture convective heat transfer model based on laboratory tests, and they analyzed the heat transfer characteristics of rough fractures within granite in detail. Based on the flow equation of the Bingham fluid flow in a single smooth inclined fracture, Luo et al[11] developed a coupled model of Bingham grout seepage and fracture deformation of a spatial rock mass fracture network. At present, researchers have successfully built numerical model of 3D discrete fracture network (DFN) in rock masses. Chen[12] generated 3D DFN models using the applied probability statistics, stochastic simulation, Monte Carlo simulation, and computer programming. Wenli et al[13] proposed a numerical DEM to reconstruct the spatial distribution of the 3D fracture network and to model the grouting slurry flow. Currently, the assumption of 'smooth surface of rock mass cracks' is widely used for the numerical simulation of grouting. The cubic law is a widely used mature diffusion theory, which describes the diffusion law of a Newtonian fluid in a single smooth parallel plate. In 1996, Zimmerman et al[14] pointed out that the single width fluid flow rate was affected by the aperture and roughness of the fracture in actual rock fractures. Dippenaar[15] discussed the effectiveness of the cubic law in different fracture types in 2016. They believed that the cubic law was not suitable for rough rock fractures due to the changes of fracture aperture and fluid flow channels that resulted from the rock fracture irregularity. In other words, the cubic law cannot be used for the rough fracture of rock masses. To solve the gap issue between the smooth parallel plate and the rough fracture surface, scholars have been made many attempts to modify the cubic law. A common method is to use the fractal theory to characterize and model the fracture surface. For instance, He-ping Xie's research team[16] has been committed to studying the distribution characteristics of rock mass fractures, and they believe that the spatial distribution of 2D fracture networks can be described by fractal dimensions, and they emphasized that the fractal fea-

Received: 5 Janury 2021 Revised: 16 March 2021
This work was supported by the Joint Fund of National Natural Science Foundation of China and Yalong River (U1765106).
First author: CUI Wei, male, born in 1977, PhD, Professor, mainly engaged in geotechnical engineering and static and dynamic analysis of hydraulic structure. E-mail: cuiwei@tju.edu.cn

tures have good self-similarity. Based on the previous work of Cui et al[17], the Weierstrass Mandelbrot (W–M) fractal function is introduced to characterize the roughness of the fracture surface. Majumdar et al[18] simulated the fracture rough surface in 1990 using the W–M function, and the results showed that the fracture surface is statistically similar to the real rough surface. In 1998, Yan et al[19] proposed the W–M fractal function expression of 3D fractures. In 2017, Jin et al[20] used the 2D W–M function to characterize the surface fracture roughness. Based on this function, they explored the influence of scale and size on the fluid flow in self-affine rough fractures. In 2019, Ju et al[21] generated the rough fracture surface using a 3D W–M function, and the correctness of the seepage model was then verified. Due to the non-Newtonian fluid characteristics of the slurry, in general, almost no research on its flow law in rough cracks is found.

In recent decades, researchers have been used successively the equivalent continuum method, the dual-medium model method and the discrete network model to simulate the fluid diffusion process in the fracture network of the rock masses[22]. A fractured rock mass is generally composed of a rock matrix and a fracture network. Compared to the fracture network portion, the permeability of the rock matrix is quite weak and it is therefore generally assumed that the rock matrix is rigid and water-impermeable material in studying the actual rock fracture grouting problem. In other words, the flow is considered to occur only in the fracture network system. In light of this, the seepage problem of fractured rock mass is essentially the seepage problem of the fracture network[23]. One of the typical results based on the discrete network model is the discrete fracture network (DFN)[24], which has good practicality in modelling the random fractures in rock masses.

To solve the above mentioned issues, this study modifies the flow equation of the viscous fluid in the rough fracture of rock masses. The two key indicators that affect the DFN properties, namely: the equivalent permeability coefficient k_e and the connectivity parameters η, as well as the grouting pressure, are studied in the grouting process for the fine rock masses using 3D numerical modelling.

2 Flow equation of viscous fluid for rough fractures within rock mass

2.1 Flow equation of viscous fluid in smooth fracture

Figure 1 shows the flow of viscous fluid in a single smooth fracture. In Fig.1, l is the fracture length; w is the fracture width; and d_f is the aperture. Based on five assumptions, Snow[25] derived the flow law of the groundwater in a single fissure (the two fracture walls are parallel smooth flat plates) --- the cubic law in 1965, and the basic expression is

$$q=\frac{gd_{\mathrm{f}}^{3}}{12v}J \tag{1}$$

where q is the single-width flow; g is the gravity acceleration; v is the kinematic viscosity coefficient; and J is the pressure ratio drop.

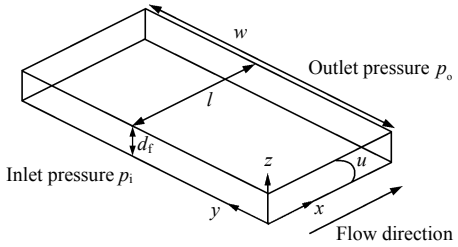

Fig. 1 A single fracture

When Bingham fluid passes through a fracture in a parallel smooth plate, the single-width flow equation is

$$q=\frac{1}{\mu}\left(\frac{\rho g d_{\mathrm{f}}^{3}}{12}J+\frac{\tau_0^{3}}{3\rho^{2}\mathrm{g}^{2}J^{2}}-\frac{\tau_0 d_{\mathrm{f}}^{2}}{4}\right) \tag{2}$$

where ρ is the density; τ_0 is the yield stress; μ is the dynamic viscosity coefficient, which can be obtained from the relation between the kinematic viscosity coefficient v and density ρ:

$$\mu=\rho v \tag{3}$$

2.2 The corrected cubic law of rough fracture

The roughness extent of a wall surface of natural fractures will inevitably cause the nonlinear behavior of fluid flow, and the rough surface would change the fracture aperture, as well as the fluid seepage path. Hence, based on the W–M fractal function, the fractal dimension D and the characteristic scale parameter G, the fracture aperture d_f, and the hydraulic gradient J in the permeability coefficient equation of Bingham fluid are modified to determine the cubic law under non-smooth conditions.

W-M function is a classic fractal function and it is also considered to represent the rough fracture surface characteristics of rock masses. The W–M function can be expressed as

$$z(x,y)=L\left(\frac{G}{L}\right)^{(D-2)}\left(\frac{\ln\gamma}{M}\right)^{\frac{1}{2}}\sum_{m=1}^{M}\sum_{n=0}^{n_{\max}}\gamma^{(D-3)n}\left\{\cos\varphi_{m,n}-\cos\left[\frac{2\pi\gamma^{n}\left(x^{2}+y^{2}\right)^{\frac{1}{2}}}{L}\cos\left(\tan^{-1}\left(\frac{y}{x}\right)-\frac{\pi m}{M}\right)+\varphi_{m,n}\right]\right\} \tag{4}$$

where x and y are the coordinates of the rough surface; z is the height of the random rough surface; L is the length of the sample; γ ($\gamma>1$) is the frequency density parameter; M is the superimposed number of rough peaks used to construct the surface; n is the frequency index; $n_{\max}$ is the upper limit of n during iteration; $\varphi_{m,n}$ is the random phase; G is the characteristic scale

parameter, which represents the profile height of the two-dimensional rough surface; D is the fractal dimension and D is a real number between 2 and 3 in the 3D fractal function. The fractal dimension D controls the complexity of the fractal curve. The larger the D value, the smaller the profile height and the higher the roughness frequency; the characteristic scale parameter G controls the height amplitude of each point on the fractal curve. Fig.2 shows the influence of different D and G on the 3D fractured fractal rough surface.

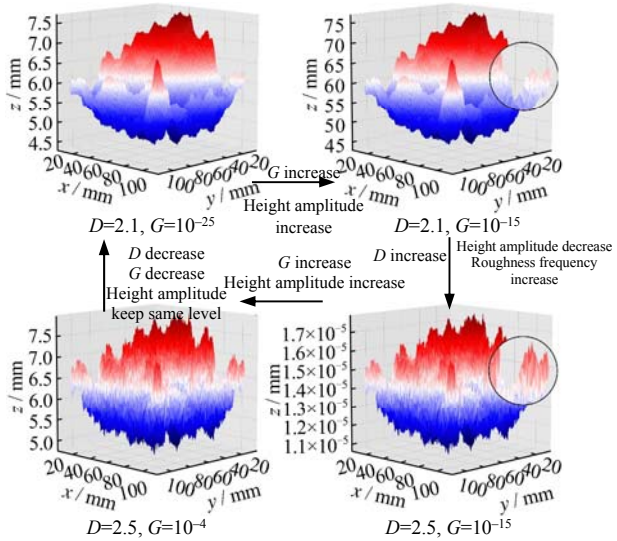

Fig. 2 3D fractal rough surfaces under different values of *D* and *G*

When the rough wall is considered, the modified equation of the single-width flow rate of Bingham fluid in fractal rock mass fractures is in the form of

$$q=\frac{\rho g\left[d_{\mathrm{f}} f(D,G)\right]^3}{12\mu}\left[Jg(D,G)\right]+\frac{{\tau_0}^3}{3\rho^2 g^2 \mu\left[Jg(D,G)\right]^2}-\frac{\tau_0\left[d_{\mathrm{f}} f(D,G)\right]^2}{4\mu} \tag{5}$$

The functions of $f(D,G)$ and $g(D,G)$ are solved using fitting method. Various D values (2.1–2.9, with an interval of 0.1) and different G values are assigned for each case. For each case, the fracture system is modeled and point cloud data is generated based on the W–M fractal function. The rough fracture surface model is then imported into the software COMSOL Multiphysics. According to the pre-defined aperture value and the normal vector of each point on the fracture surface, area integration of all points on the fracture surface is performed and the true average aperture value of the fractal fracture is determined, and the f value is then calculated afterward. Similarly, the true average hydraulic gradient value can be estimated for the fractal fracture, and the g value is then derived for each case. The form of $f(D,G)$ and $g(D,G)$ functions are

$$f,g(D,G)=\left\{1+\exp\left[\frac{\lg G-\left(y_1+A_1 \mathrm{e}^{\frac{2-D}{A_2}}\right)}{t_1+A_3 \mathrm{e}^{\frac{2-D}{A_4}}}\right]\right\}^{-1} \tag{6}$$

According to the relations among D, y_0, and t_0, the values of y_1, A_1, A_2, t_1, A_3, and A_4 are fitted and these associated values are shown in Table 1. The curves of $f(D,G)$ and $g(D,G)$ functions and the contours of corresponding influence factors are shown in Fig.3. An S-shaped distribution is observed under the influence of D and lg$G$ on the $f(D,G)$ and $g(D,G)$ functions.

Table 1 Fitted values of the fractal correction function of W–M

Fitting parameter	$f(D,G)$	$g(D,G)$
y_1	–0.82	–0.85
t_1	–1.88	–2.31
A_1	–33.74	–16.12
A_2	0.11	0.19
A_3	3.75	3.05
A_4	1.51	4.31
R^2	0.90	0.79

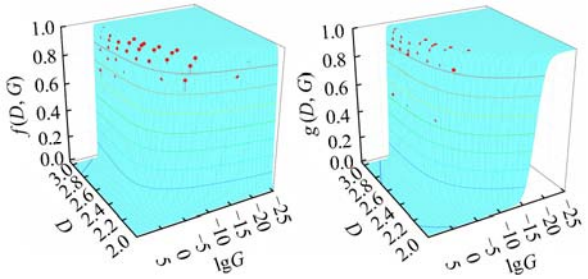

(a) $f(D,G)$ (b) $g(D,G)$

Fig. 3 Corrected function *f*(*D*,*G*) and *g*(*D*,*G*) curves and the contours with influence factors

2.3 Verification of the modified cubic law of rough fractures

As shown in Fig.4, a grouting visualization test system is used for the single micro-fracture test in this study. During the test process, the test pressure is increased by a compressor, and a pressure stabilizer is used to provide a constant pressure, which is used to push the silica sol solution for grouting purposes from a solution bottle. Through the pressure sensor and the ELVEFLOW software, the pressure changes at both ends and the flow changes within the micro-cracks are recorded in real time during the test.

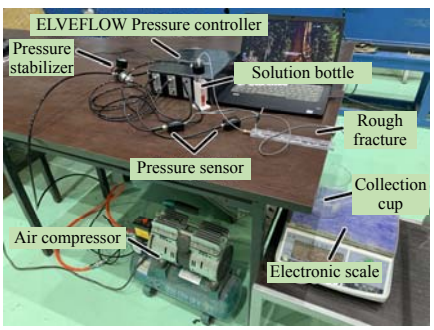

Fig. 4 Grouting visualization test system

In the tests, four fractures are generated from 3D printing. The fracture apertures are 1.2 mm and the characteristic scale parameter G are all 0.03 (lg$G$ = –1.5), the fractal dimensions D are 2.7, 2.8, 2.9, and

3.0 for the four fractures, respectively. The fracture surface is smooth when D = 3.0, that is, the parallel plate model. Fig.5 presents an omnidirectional view of one fracture and the fracture dimension. To measure the flow rate of a single fracture with a single width, a 2 mm opening is reserved at the front end of the rough fracture as a connector for the grouting pressure pipe.

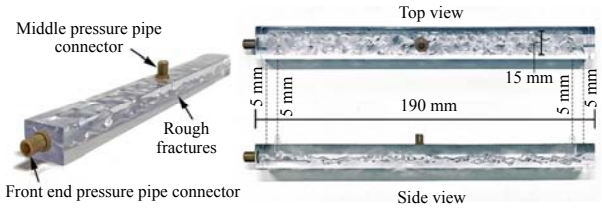

(a) Rough fracture (b) Overall dimension

Fig. 5 Rough fracture and overall dimensions

For each prepared fracture from the 3D printing, eight tests were conducted on each fracture and the injection pressure was maintained from 25 to 200 kPa with an interval of 25 kPa at the front end of the fracture. The single-width flow rate through each crack can be obtained for the same time interval t. The correctness of the W–M fractal theory can be verified through flow rate comparison between the measured single-width flow and the derived results from Eq.(5). Fig.6 shows the comparison between the test values and the theoretical values of the single-width flow through each fracture under different inlet pressures, and the results show a good agreement between the test results and the derived results. Under the same inlet pressure, it is found that the single-width flow rate considering the rough fracture is lower than that from the calculation result for the parallel plate model (D = 3.0). The flow rate decreases more obviously as the fracture roughness increases. It is therefore necessary to modify the cubic law for the rough fracture. In addition, it is found from Fig.6 that, for most of the cases, the test values are slightly lower than that of the theoretical single-width flow rate. One of the possible reasons for this phenomenon could be the errors caused by the residual bubbles in the fractures.

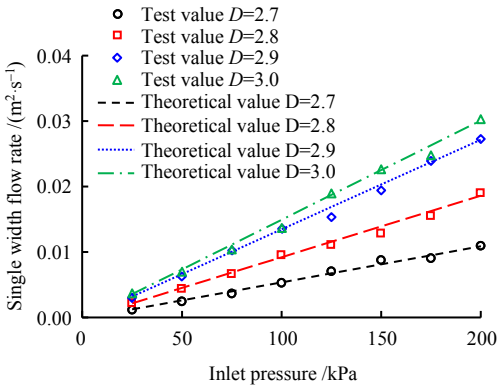

Fig. 6 Comparison between the experimental data and theoretical values for a single width flow rate

3 Numerical modelling of grouting process in fractured rock mass

3.1 Characterization of fracture network

Using the open-source code dfnWorks, three fracture network models are generated (F-1, F-2 and F-3) as shown in Fig.7. All fractures within the model are stochastically generated in a cuboid volume with 3.0 m length and width and 10.0 m height. The fracture is modeled in an octagonal shape. The total number of fractures is 197, 174, and 185 for the F-1, F-2 and F-3 DFN model, respectively. The fracture apertures are defined as 1, 2 and 3 mm for the tree DFN models, respectively. The roughness frequency and height amplitude of fracture surface are defined by the fractal dimension D and the characteristic scale parameter G, respectively. The G values of the three DFN models are all 0.03 (lg$G$ = –1.5), and the D values are 2.7, 2.8 and 2.9, which corresponding to the f values of 0.79, 0.89 and 0.98 and the g values of 0.72, 0.87 and 0.96, respectively. In this condition, the surface roughness of the fractal fracture becomes smaller and smaller. The distribution of the fracture trace length is followed by the exponential function:

$$f = \alpha e^{-\alpha x} \tag{7}$$

where f is the probability density distribution of the fracture trace length; α is the exponential function parameter; and x is the fracture trace length.

Each DFN model contains four groups of fractures with different quantified proportions, the ratios of the four groups are 0.3, 0.2, 0.2, 0.3 (the summation of the four ratios is 1.0), and the exponential function parameters of each fracture group are assigned with different values.

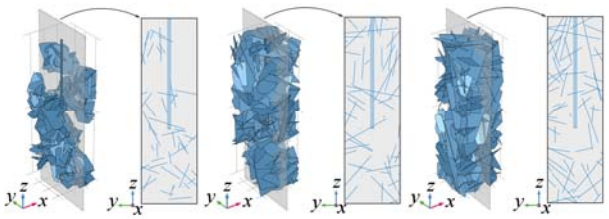

(a) F-1 (b) F-2 (c) F-3

Fig. 7 Fracture network model

Based on the two key indicators that affect the properties of the DFN model, namely the equivalent permeability coefficient k_e and the connectivity parameter η, the DFN models are then evaluated in terms of k_e and η.

3.1.1 Connectivity

Based on the viewpoint of Leung et al.[26], in this study, the fracture trace length and the connectivity of the DFN model are combined for the purpose of evaluating the connectivity parameter η of the 2D discrete fracture network:

$$\eta = \sqrt{A\varepsilon_{\text{mean}}\rho_{\text{seg}}}$$

$$\varepsilon_{\text{mean}} = \rho_{\text{A}}\left(\frac{\bar{l}^2}{2}\right)^2,\ \rho_{\text{seg}} = \frac{N_{\text{F}} + 2N_{\text{node}}}{A} \tag{8}$$

where $\varepsilon_{\text{mean}}$ and ρ_{seg} are the mean density and segment density of the 2D DFN model, respectively; A is the area of the entire region; ρ_{A} is the fracture density within the region, that is, the fracture number contained in the unit area; $\bar{l}^2$ is the square of the average fracture trace length; N_F is the total fracture number; and N_{node} is the number of the DFN intersection points.

For the DFN models F-1, F-2, and F-3, 11 planes are cut along the y-z plane at a 0.3 m interval (i.e., x = 0, x = ±0.3,..., x =±1.5) and the associated connectivity parameter η_i are then calculated for each cut planes. Taking the mean value of η_1–η_{11}, the connectivity parameter η are 1.65, 2.87, and 2.03 for F-1, F-2, and F-3, respectively.

3.1.2 Estimation of equivalent permeability coefficient based on W–M theory

Based on a single smooth fracture and the W–M fractal theory, the permeability coefficient of a single fracture is explored firstly considering the fracture roughness. Subsequently, the equivalent permeability coefficient of the DFN model is then derived in a similar fashion. Based on a simulation code COMSOL Multiphysics, the equivalent permeability coefficient of the DFN can be obtained through Darcy's law, which can be regarded as an equivalent combined value of the permeability coefficients for all the single fracture.

Darcy's law of the DFN can be

$$Q = A' \frac{k_{\text{e}}}{\mu} \frac{\Delta p'}{L'} \tag{9}$$

where Q is the total fluid volume that passing through the DFN per second; A' is the cross-sectional area that perpendicular to the fluid flow direction; $\Delta p'$ is the water pressure difference between the inlet and the outlet boundary of the DFN model; L' is the length of the DFN in the direction of fluid flow; and k_{e} is the equivalent permeability coefficient.

The equivalent permeability coefficient k_{e} of the DFN can be derived from Eq.(9). Substituting the DFN models of the F-1, F-2 and F-3 into E.(9) for the calculation, the equivalent permeability coefficients k_{e} are 1.73×10^{-4}, 3.84×10^{-3} m/s and 2.72×10^{-2} m/s for the three DFN models, respectively. The three DFN models (F-1, F-2 and F-3) are then categorized as a weakly permeable layer, a medium permeable layer and a strongly permeable layer.

3.2 Experimental study on viscous fluid behavior

3.2.1 Rheological test of silica sol

The size of micro-fractures in the rock mass is relatively small, which caused the injection issue (i.e, difficult to push the cement into the fracture) of the commonly used cement-based grouting materials. To avoid this issue, in this study, silica sol grouting material is used and the silica sol's density is comparable to water and with a low viscosity. The silica sol can be injected smoothly into the micro fractures, even for a fracture with width less than 0.5 mm[27]. According to previous studies[28–29], Bingham constitutive relation is used in this study to describe the stress–strain relation of silica sol and the constitutive model can be expressed as Eq.(10):

$$\tau = \tau_0 + \mu\gamma \tag{10}$$

where τ is the shear stress (Pa); τ_0 is the yield stress (Pa); and γ is the shear rate (s^{-1}).

The NDJ-8S digital rotary viscometer was used to measure the yield stress of the silica sol in the fresh state. The yield stress was 3 Pa and the viscosity μ was 5 mPa • s. Therefore, the constitutive equation of silica sol in the fresh state is

$$\tau = 3 + 0.005\gamma \tag{11}$$

3.2.2 Time-varying viscosity measurement

It is known that fast coagulation ability is another characteristic of silica sol. Based on the rheological tests, another equal amount of silica sol solution was prepared to explore the time-varying characteristics of the viscosity, as shown in Fig.8. It can be derived from Fig.8 that the equation of the viscosity varying with time

$$\mu = 3.763\ 44\mathrm{e}^{0.060\ 22t} \tag{12}$$

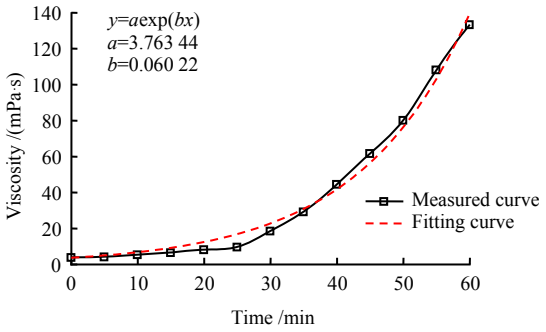

Fig. 8 Viscosity–time curve of silica sol

3.3 Modelling cases and input parameters

The 3D DFN models F-1, F-2 and F-3 that were generated using the software dfnWorks have 231 138, 407 095, and 531 305 triangular facets, respectively. Fig.9 gives the boundary conditions of the modelling. The top surface of the grouting pipe is defined as the pressure input boundary, and the side and bottom surfaces of the entire rock mass fracture network are the pressure output boundaries.

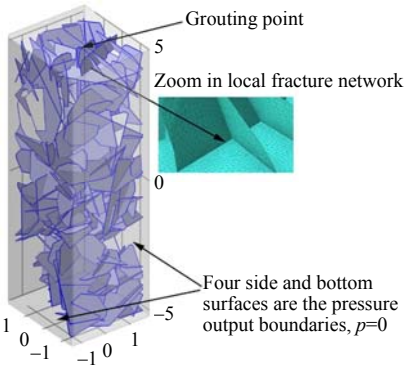

Fig. 9 Boundary condition setting

Two working cases are set herein. Case 1: vary the behavior of the DFN model and the simulated grouting pressure is all set as 0.5 MPa. Eqs.(11) and (12) are used to define the rheological and time varying characteristics of silica sol. In other words, Case 1 is designed to study the influence of different of equivalent permeability coefficient and connectivity parameters on the viscous fluid flow within a micro fracture DFN characteristics. Case 2: change the grouting pressure and based on the same DFN model of F-2. In this case, the equivalent permeability coefficient and connectivity parameters keep the same, and the values of k_e and η are 3.84×10^{-3} m/s and 2.87, respectively. The effect of different grouting pressures (1.0, 2.0 and 4.0 MPa) on the viscous fluid flow is investigated for the micro-fracture DFN model.

4 Result analysis and discussion

4.1 DFN characteristics

Figure 10 shows the diffusion behavior of time varying viscous fluids in DFN model of F-1, F-2 and F-3. Based on the horizontal diffusion process analysis for each DFN model, it is seen from Fig.10 that the connectivity parameter of the DFN model is an important indicator that affects the fluid diffusion process. In other words, the fluid always flows through the region with relatively good local connectivity first and then diffuses into the area with relatively poor local connectivity.

In addition, it is seen that the smaller the t value, the faster the fluid diffusion process, and the larger the t value, the slower the fluid diffusion process. This observation is caused by the fact that the silica sol is a time-varying viscous fluid and the slurry viscosity increases as hydration time increases. The increasing of fluid viscosity would lead to the obvious condense phenomenon. Under the same grouting pressure condition, the fluid diffusion speed decreases largely, which increases the grouting difficulty of fractures within rock masses.

Based on the comparison of the diffusion process for the three DFN models, it is seen from Fig.10 that the higher the equivalent permeability coefficient of the DFN model, the faster the fluid diffusion rate. The connectivity parameter of F-3 model (η = 2.03) is smaller than that of F-2 model (η = 2.87). Compared with F-3 model when t = 150 s, the slurry in F-2 model has flowed through a large portion of the fracture network system; however, compared with F-2 model when t = 250 s, the fluid in F-3 model has flowed through most areas of the fracture network system, which indicates that the permeability of rock masses determines the range of grouting diffusion. Again, connectivity plays an important factor in the grouting process, but only works for a short-term and in a partial role during the whole process. Similarly, it should be mentioned that the above statements are only valid for fracture networks with strong stochastic and a large number of fractures.

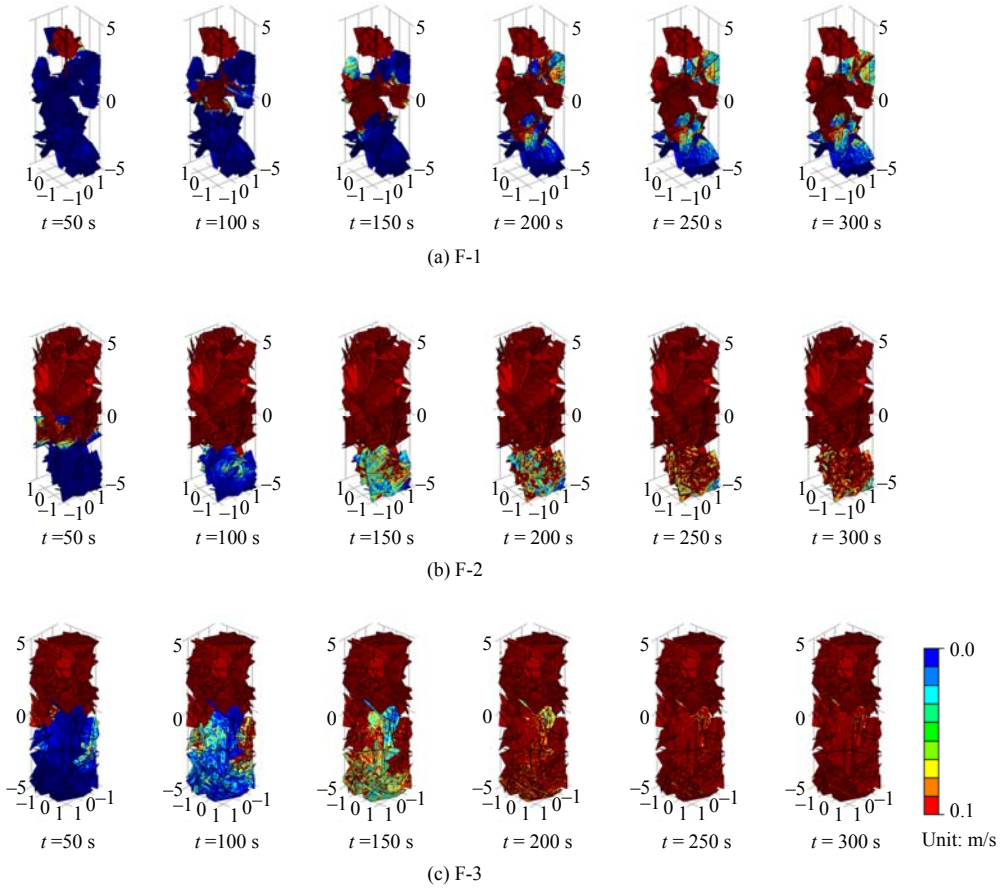

Fig. 10 Fluid diffusion process

After the transient numerical simulation, the corresponding radius r value is then calculated by $r = \sqrt{x^2 + y^2}$ based on the x and y coordinates of each node. Subsequently, the average velocity of each component is calculated and the average velocity contour of the entire fracture area under the three modelling cases is then generated. Additionally, the mean steady-state velocity of the silica sol fluid flow is also generated for the cut plane of $x = 0$ section, as shown in Fig.11.

From Fig.11, it is seen that the closer distance to the grouting pipe location, the higher the fluid flow velocity in the fracture network system. For F-3 model, for instance, it is observed that high velocity area is located in a triangle area near the grouting point, and the average velocity of the viscous fluid can reach up to 2 m/s in the micro fracture system. In addition, the average fluid velocity is very small when the z value is small or the r value is large, basically the flow velocity is smaller than 0.25 m/s. This observation indicates that the slurry fluidity is very slow in such areas. It reflects, to a certain extent, the limitation of grouting in the diffusion range.

In addition, by observing the overall average velocity contour and the section average velocity distribution, it is found that the above-mentioned statement is not always true. Again, taking F-3 model as an example, for some points with the same r value, it is seen that some points have a smaller z value, but the average velocity is higher than that from some points with larger z value. This observation is mainly determined by the connectivity parameters of the DFN model, which reveals that the connectivity of some points with smaller z value is larger than that of the points with larger z values. In this manner, the fluid is relatively easier to flow and reach higher flow velocity.

From the comparison of Fig.11 for different DFN models, it is shown that the larger the equivalent permeability coefficient of the DFN model, the faster the fluid flow rate for the whole DFN model, in which the fracture aperture and surface roughness play a key role in determining the flow velocity rate. From the overall and section velocity contours of F-3 model, it is found that the red area is larger than that of F-1 model and F-2 model. This phenomenon indicates that the permeability of rock mass is the decisive factor in determining the grout diffusion range, which becomes even more accurate for the DFN with more fractures. The reason could result from the large variability and randomness in fracture directions, which will contribute to much better connectivity of the DFN system.

4.2 Grouting pressure

In the same manner, the overall regional average velocity (3D) and the average velocity at $x = 0$ section (2D) plane are generated for the F-2 DFN model under the grouting pressure of 1.0, 2.0 and 4.0 MPa, as shown in Fig.12. It is seen from Fig.12 that the slurry flow velocity increases as the grouting pressure increases. The larger the grouting pressure, the larger the range of the red area. For all the three DFN cases, the outline shape of velocity contours are consistent, which means that, if other conditions are the same, the increase of grouting pressure will boost the grout diffusion speed, making it easier for the slurry to diffuse to the areas far away from the grouting point and with poor local connectivity. According to the modelling results, a 2.0 MPa grouting pressure is suitable for F-2 model (the equivalent permeability coefficient is 10^{-3}, as a medium permeable layer).

A point A (1, 1, 3) is selected randomly in the F-2 model and the velocity of the grout at this point is tracked at t = 0–300 s (with an interval of 50 s) under different grouting pressures. Fig.13 shows the curves of time–velocity. It is seen from Fig.13 that slurry spreading speeds increase in approximately the same proportion as the increase of the grouting pressure for a certain point within the fracture system. When the grouting pressure is 4.0 MPa, for instance at any time, the slurry spreading speed at this point is roughly 8 times the speed when the grouting pressure is 0.5 MPa. This observation is also consistent with the phenomenon shown in Fig.12.

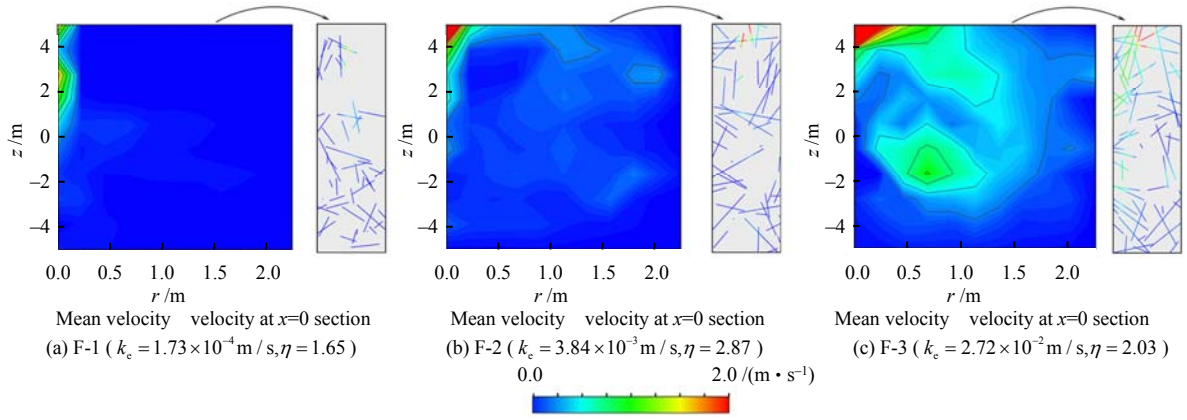

Fig. 11 Mean velocity contours of the overall and sectional planes

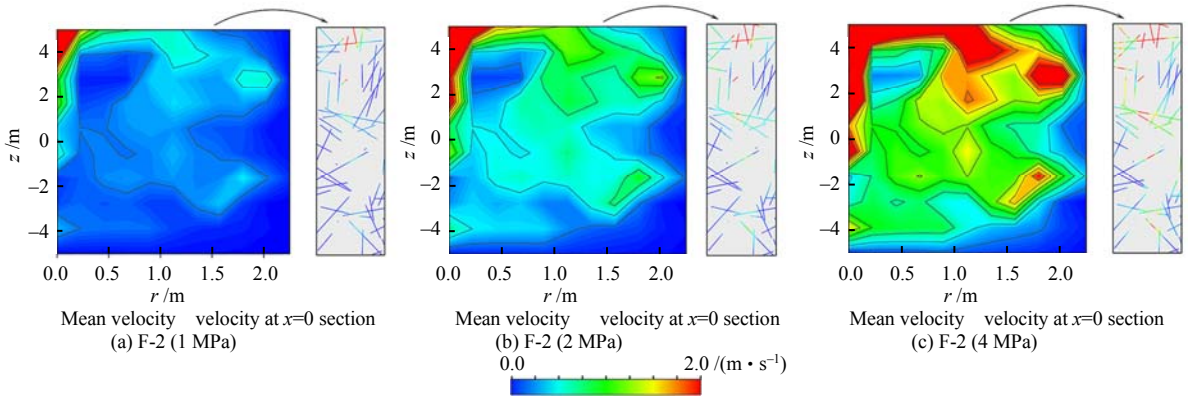

Fig. 12 Mean velocity contours of the overall and sectional planes for F-2 under different grouting pressures

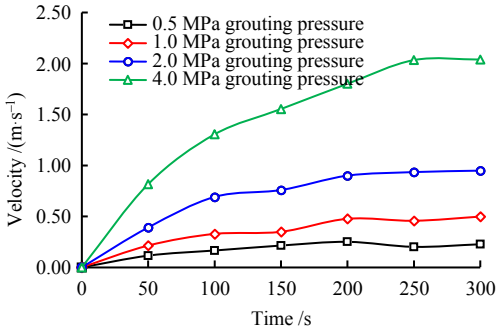

Fig. 13 Velocity–time curves at point *A* (1,1,3) under different grouting pressures

5 Conclusion

Assuming the size of grout particles is smaller than the fracture width, based on the modified cubic law of Bingham viscous fluid flowing in rough rock mass fractures, rock mass discrete fracture network (DFN) model is then generated in this study. Through varying the DFN's characteristic parameters (such as the permeability coefficient and connectivity) and injection pressure, the grouting process of viscous fluid was simulated and studied for the rock mass with micro fractures. The main conclusions are as follows:

(1) The cubic law does not consider the fracture roughness of actual rock masses. The fracture aperture and hydraulic slope are corrected in the cubic law, a modified cubic law is obtained for the viscous fluid with rough fracture, which agreed reasonably well with the results of the single fracture grouting test.

(2) The characteristics of DFN have a controlling role in the grouting process. Among them, the equivalent permeability coefficient determines the range of the grouting diffusion, and the connectivity of the fracture network significantly affects the grout flow velocity and diffusion process within a local area.

(3) The increasing grouting pressure will change the grout diffusion speed, making it easier for the grout to diffuse to the areas far away from the grouting point and with poor local connectivity. However, excessive grouting pressure may lead to the fracture opening and even damage the rock mass. According to the modelling results, a 2.0 MPa grouting pressure is suitable for F-2 model (the equivalent permeability coefficient is 10^{-3}, as a medium permeable layer).

It is known that many factors can affect the grout diffusion in fractured rock masses, including the rock composition, grout particle size, local fracture connectivity. Due to the limitation of the research method in this study, those influence factors will be discussed in-depth in the future studies.

References

[1] YANG Mi-jia, HE Yong-nian, CHEN Ming-xiong. Grouting seepage law in fractured rock mass network[J]. Journal of Hydraulic Engineering, 2001, 32(7): 41–46.

[2] FONDRIEST M, ARETUSINI S, DI TORO G. Fracturing and rock pulverization along an exhumed seismogenic fault zone in dolostones: the Foiana Fault Zone (Southern Alps, Italy)[J]. Tectonophysics, 2015, 654(8): 56–74.

[3] WANG K, WANG L, REN B. Understanding the effect of cementitious grouting pressure on micro-fracture permeability for rock reinforcement underground: a lab study[J]. Energies, 2020, 13(16): 4225.

[4] ZHANG J, PEI X, WANG W, et al. Hydration process and rheological properties of cementitious grouting material[J]. Construction and Building Materials, 2017, 139: 221–231.

[5] WANG Y H, YANG P, LI Z T, et al. Experimental-numerical investigation on grout diffusion and washout in rough rock fractures under flowing water[J]. Computers and Geotechnics, 2020, 126: 103717.

[6] RUAN Wen-jun. Research on diffusion of grouting and basic properties of grouts[J]. Chinese Journal of Geotechnical Engineering, 2005, 27(1): 69–73.

[7] RUAN Wen-jun. Spreading model of grouting in rock mass fissures based on time-dependent behavior of viscosity of cement-based grouts[J]. Chinese Journal of Rock Mechanics and Engineering, 2005, 24(15): 2709–2714.

[8] GUSTAFSON G, CLAESSON J, FRANSSON A. Steering parameters for rock grouting[J]. Journal of Applied Mathematics, 2013(1): 1–9.

[9] KOBAYASHI S, STILLE H, GUSTAFSON G, et al. Real

time grouting control method: development and application using Äspö HRL data[J]. Swedish Nuclear Fuel and Waste Management Company, Stockholm, Sweden, 2008, 60(1): 73–73.

[10] GAO Xue-feng, ZHANG Yan-jun, HUANG Yi-bin. Numerical simulation of convective heat transfer characteristics of a rough single fracture in granite[J]. Rock and Soil Mechanics, 2020, 41(5): 1761−1769.

[11] LUO Ping-ping, CHEN Lei, ZOU Zheng-sheng. Numerical simulation of grouting in space fracture network of rock mass[J]. Chinese Journal of Geotechnical Engineering, 2007, 29(12): 1844–1848.

[12] CHEN Jian-ping. 3D net work numerical modeling technique for random discontinuities of rock mass[J]. Chinese Journal of Geotechnical Engineering, 2001, 23(4): 397–402.

[13] YAO W L, MOSTAFA S, ZHEN Y, et al. Assessment of fracture characteristics controlling fluid flow performance in discrete fracture networks (DFN)[J]. Journal of Petroleum Science and Engineering, 2019, 178: 1104–1111.

[14] ZIMMERMAN R W, BODVARSSON G S. Hydraulic conductivity of rock fractures[J]. Transport in Porous Media, 1996, 23(1): 1–30.

[15] DIPPENAAR M A, VAN ROOY J L. On the cubic law and variably saturated flow through discrete open rough-walled discontinuities[J]. International Journal of Rock Mechanics and Mining Sciences, 2016, 89: 200–211.

[16] WANG Zhi-guo, ZHOU Hong-wei, XIE He-ping. Research on fractal characterization of mined crack network evolution in overburden rock stratum under deep mining[J]. Rock and Soil Mechanics, 2009, 30(8): 2403−2408.

[17] CUI Wei, ZOU Xu, LI Zheng. Seepage diffusion in a fractal single micro-rock-fracture under multiple experimental cases[J]. Rock and Soil Mechanics, 2020, 41(11): 3553−3562.

[18] MAJUMDAR A, TIEN C L. Fractal characterization and simulation of rough surfaces[J]. Wear, 1990, 136(2): 313–327.

[19] YAN W, KOMVOPOULOS K. Contact analysis of elastic-plastic fractal surfaces[J]. Journal of Applied Physics, 1998, 84(7): 3617–3624.

[20] JIN Y, DONG J, ZHANG X, et al. Scale and size effects on fluid flow through self-affine rough fractures[J]. International Journal of Heat and Mass Transfer, 2017, 105: 443–451.

[21] JU Y, DONG J, GAO F, et al. Evaluation of water permeability of rough fractures based on a self-affine fractal model and optimized segmentation algorithm[J]. Advances in Water Resources, 2019, 129: 99–111.

[22] LEMOS J. A distinct element model for dynamic analysis of jointed rock with application to dam foundation and fault motion[D]. [S. l.]: University of Minnesota, 1987.

[23] YAO C, HE C, YAN J, et al. A novel numerical model for fluid flow in 3D fractured porous media based on an equivalent matrix-fracture network[J]. Geofluids, 2019. DOI: 10.1155/2019/9736729.

[24] LONG J C S, REMER J S, WILSON C R, et al. Porous media equivalents for networks of discontinuous fractures[J]. Water Resources Research, 1982, 18(3): 645–658.

[25] EKER E, AKIN S. Lattice Boltzmann simulation of fluid flow in synthetic fractures[J]. Transport in Porous Media, 2006, 65(3): 363–384.

[26] LEUNG C T O, ZIMMERMAN R W. Estimating the hydraulic conductivity of two-dimensional fracture networks using network geometric properties[J]. Transport in Porous Media, 2012, 93(3): 777–797.

[27] DUAN Xiao-na, SUN Yang-yang, ZHANG Hai-hong, et al. Research progress and application of silica sol[J]. Bulletin of the Chinese Ceramic Society, 2014, 33(4): 836−840.

[28] YZIQUEL F, CARREAU P J, MOAN M, et al. Rheological modeling of concentrated colloidal suspensions[J]. Journal of Non-Newtonian Fluid Mechanics, 1999, 86(1-2): 133–155.

[29] GEHIN C, PERSELLO J, CHARRAUT D, et al. Electrorheological properties and microstructure of silica suspensions[J]. Journal of Colloid and Interface Science, 2004, 273(2): 658–667.